Proceedings of the
Annual Stability Conference
Structural Stability Research Council
Louisville, Kentucky, April 1-4, 2025

Numerical modeling of the post-earthquake fire performance of cold-formed steel members

Yu Niu[1], Zhanjie Li[2], Sean Enright[3], Joshua Dillard[4], Tara Hutchinson[5], Richard Emberley[6], Brian Meacham[7], Thomas Gernay[8]

Abstract
The objective of this paper is to investigate the post-earthquake thermal-mechanical response of cold-formed steel (CFS) members. A 10-story cold-formed steel building (CFS-NHERI) will undergo seismic tests, followed by post-earthquake live fire tests. To support the fire test setup, computational models are developed to simulate the impact of varying post-earthquake damage levels on the fire response of the structure. As a panelized system, damage to different finish and nonstructural systems significantly affects the thermal behavior and load-bearing capacity of the CFS components. The computational models integrate the modeling capability in CUFSM and SAFIR for the elastic buckling, heat transfer, and transient structural analysis under fire. A parametric analysis considering different seismic damage levels is conducted to study the buckling and strength behavior of the CFS members under fire-induced nonuniform temperature fields. These pre-test models inform the duration and severity of the fire tests to maintain structural stability while achieving substantial thermal loading on the CFS load-bearing system. They also provide guidance for the sensor layout plan for the fire tests. This study advances methods for fire resilience of thin-walled CFS structures under multi-hazard scenarios.

1. Introduction
Cold-formed steel (CFS) structures play a pivotal role in modern construction, particularly in low- to mid-rise buildings, due to their high strength-to-weight ratio, ease of assembly, and versatility. CFS framing systems are widely used in both non-load-bearing applications, such as partition walls, and load-bearing structural roles. To enhance their lateral resistance to seismic and wind loads, CFS framing walls are often supplemented with sheathing materials such as oriented strand board, steel sheet, gypsum-steel composites, or steel strap bracing. The behaviors of CFS framing walls have been extensively studied under lateral forces from earthquakes or wind (Liu et al., 2014; Ye et al., 2015; Zhang et al., 2024), axial loads from upper stories (Miller & Pekoz, 1993; L. C.

[1] PhD Student, Johns Hopkins University, yniu11@jhu.edu
[2] Professor, SUNY Polytechnic Institute, zhanjie.li@sunypoly.edu
[3] Master's Student, Johns Hopkins University, senrigh3@jhu.edu
[4] Master's Student, Johns Hopkins University, jdillar6@jh.edu
[5] Professor, University of California San Diego, tahutchinson@ucsd.edu
[6] Associate Professor, California Polytechnic State University, emberle@calpoly.edu
[7] PhD, Meacham Associates, brian.meacham@meachamassociates.com
[8] Assistant Professor, Johns Hopkins University, tgernay@jhu.edu

M. Vieira Jr et al., 2011), and combined axial and lateral loading (Peterman & Schafer, 2014). These studies have highlighted key failure mechanisms and revealed the role of structural and nonstructural sheathing materials in enhancing the strength, stiffness, and overall stability of CFS systems. Similarly, advances have been made in the fire performance of CFS framing walls, particularly in understanding thermal-structural interactions through experimental and numerical studies (Abreu et al., 2020; Feng & Wang, 2005; Ni et al., 2022; Vy et al., 2023; Yan & Gernay, 2022). CFS members inside the framing walls subjected to elevated temperatures exhibit complex responses, including nonuniform temperature distributions, thermal bowing, and shifts in the neutral axis, which can amplify structural demands and exacerbate cross-sectional instabilities.

In multi-hazard scenarios, such as earthquakes followed by fires, understanding the thermal-mechanical response of CFS members is critical for ensuring structural safety and resilience. Post-earthquake damage can significantly alter the fire performance of CFS systems, with damage to finish and nonstructural components influencing heat transfer and load-bearing capacity of the structural elements. Protective materials, such as gypsum board, are critical in mitigating heat transfer to structural components, preserving their load-bearing capacity during fire exposure (Chen et al., 2020). Cross-sectional instabilities, including local and distortional buckling, may be further compounded by the residual stresses and deformations induced by seismic activity.

In 2016, full-scale fire tests were performed on an earthquake damaged, 6-story CFS building constructed on the Large High-Performance Outdoor Shake Table (LHPOST) at UC San Diego (Hutchinson et al., 2021). The test specimen, designed to meet code provisions for a location near downtown Los Angeles, underwent a series of earthquake simulations followed by six short-duration compartment fire tests on two different floors. The fire test compartments were constructed to represent 60-minute fire resistance rated construction in its undamaged condition. Pool fires were used to generate post-flashover conditions with peak compartment temperatures reaching 800°C to 1,000°C, but for a limited duration, with a target of less than 2 MW for 20 minutes or less (Kamath et al., 2017). The fire tests revealed significant degradation of fire-rated gypsum boards, stiffness loss in floor sheathing, and failures in fire-rated door assemblies due to earthquake-induced damage. Despite sustaining extreme damage, including a full soft-story mechanism at Level 2 during a near-fault earthquake test, the structure resisted collapse through load redistribution via tie-down rods and compression pack systems. These findings underscored the potential vulnerabilities of CFS systems in sequential earthquake and fire events.

The 10-story 'CFS10' tests look to expand knowledge of post-earthquake performance of CFS construction, in this case by exposing the test specimen to longer duration post-flashover fire conditions, and further exploring the structural fire performance of the specimen, and the potential for smoke and fire spread inside and outside of the specimen. This test series will also feature inclusion of horizontal and vertical pipe runs, representative of fire sprinkler systems and fuel gas systems, as was done in the building nonstructural components test series in 2012 (Meacham, 2016). The presence of the piping is intended to provide fragility data for the earthquake motion tests and provide means to test various firestop systems in floor and wall penetrations. The test specimen will also feature an interior stair, which was not present in the CFS-HUD testing in 2016. These tests will also present an opportunity for first responders to witness earthquake and post-earthquake fire damage, and to conduct limited training exercises in the test specimen.

Within this CFS10 program, this paper focuses on computational modeling of the response of CFS members in the fire compartment. A computational framework is built to support such analyses by integrating the tools CUFSM (Adany, 2006; Li & Schafer, 2010), for analyzing cross-sectional instabilities in CFS members, and SAFIR (Franssen & Gernay, 2017), for heat transfer and transient thermal-mechanical analysis. This combination facilitates model construction and enables capturing the nonlinear response and the instabilities under fire. Parametric studies are then conducted to investigate how different seismic damage levels influence the thermal and structural response of the CFS members, including under transient nonuniform temperature fields.

2. Description of the building and CFS stud under study

The multi-university-industry project *Seismic Resiliency of Repetitively Framed Mid-Rise Cold-Formed Steel Buildings*, funded through the National Science Foundation (NSF), referred to as CFS-NHERI, was undertaken to advance knowledge of the seismic performance of mid-rise CFS-framed building systems. CFS-NHERI aims to support improvements in seismic design codes for such systems and expand their use to mid-rise buildings. Works so far in the project have provided insights into the behavior of connections, components and subsystems (Castaneda, 2022; Singh et al., 2022a, 2022b; Zhang et al., 2022). CFS10 (*CFS10*, 2025) is the capstone to this effort, with the goal of demonstrating the advancement of CFS seismic detailing at full-scale via construction and earthquake testing of a 10-story fully CFS-framed building attached to the UC San Diego outdoor shake table (esec.ucsd.edu). CFS10 builds upon successful full-scale building programs of the 2-story CFS-NEES (Peterman et al., 2016) and 6-story CFS-HUD programs (Hutchinson et al., 2021). CFS10 is a landmark building specimen designed beyond current code-limits with advances in steel sheathed shear walls and heavy chord stud details proofed in complementary component test programs. This test specimen embraces a variety of construction modalities including 2D panelized construction and 3D volumetric construction methods. At the time of preparation of the present paper, CFS10 was under construction, having completed 6-stories of structural construction (Fig.1a). Ultimately this test building will be 10-stories (Fig.1b) and provide full-scale system-level benchmark test data for a state-of-the-art CFS building under sequentially damaging multi-directional earthquake input. Complimentary live fire tests (Fig.1c) led by Cal Poly San Luis Obispo will facilitate additional understanding of the thermal and smoke spread within seismically damaged compartments. The fire tests will be conducted, post seismic testing, in compartments located on the third, sixth, and ninth floors.

This study focuses on the structural fire response of the gravity studs in the shear walls of the third-floor compartment (Fig.1d). The shear walls are made of repetitive framing of cold-formed steel studs and tracks, with a steel sheathing on the exterior side of the compartment, and lined with gypsum boards. In the third-floor fire compartment, the shear walls use studs with a cross-section of 600S162-54(50) and a length of 3048 mm (120 inches). Fasteners are placed at a spacing of 304.8 mm (12 inches) along the interior of the sheathing panel. To evaluate the forces in the studs during the fire tests, two load cases are considered. Load Case 1 (LC1) considers the dead load only with a factor 1.0, to represent the expected force from building dead load. Load Case 2 (LC2) includes 1.2 times the dead load plus 0.5 times the live load in accordance with ASCE 7 for fire design (*ASCE/SEI 7-22*, 2022). The maximum axial force in the gravity studs among the four fire-exposed shear walls in the compartment is 2882 N for Load Case 1 and 5191 N for Load Case 2. These forces are obtained from a numerical model in an OpenSeesPy framework using a finite element (FE) model with nonlinear displacement-based beam-column line elements.

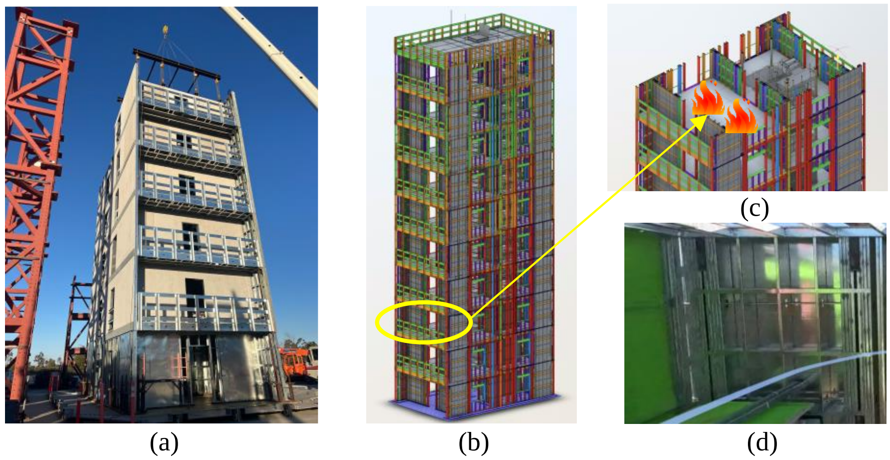

Fig. 1: 10-story cold-formed steel building specimen, coined CFS10: (a) Under construction (January 9, 2025 at 6-levels) at the LHPOST6 facility in San Diego, (b) Revit model rendering upon completion (estimated March 2025), (c) sectional view steel sheathed shearwalls (vertical lateral force resisting system) and (d) shear wall in the fire compartment showing the studs under study, before covering by the plasterboard.

A first evaluation of the strength of the 600S162-54(50) CFS stud was performed using the Direct Strength Method (DSM) (Schafer, 2008) in the CUFSM software (Fig. 2). The evaluation is conducted for various uniform elevated temperature conditions by adjusting the material properties with the appropriate retention factors (Yan et al., 2021). In addition, the restraint effect from the sheathing is considered using springs placed at intervals of 304.8 mm (corresponding to the fastener position). The spring stiffness was taken as k_x = 35025 N/m and k_z = 7 N/m. These values are conservatively lower than reported data for fastener-stud-sheathing stiffness at ambient temperature (Peterman & Schafer, 2012; L. C. Vieira Jr & Schafer, 2012) to account in a simplified manner for temperature degradation; future works will aim to incorporate the temperature-dependency of this stiffness explicitly. A significant unknown for the test program lies in the integrity of the gypsum sheathing and sheathing-to-stud connection following the seismic test and throughout the fire test. Therefore, the DSM evaluation was conducted under three assumptions: (i) the restraint is intact (*L120_Springs*), (ii) the partially degraded sheathing fastener provides only half of the restraint stiffness (*L120_HalfStiff*), and (iii) the sheathing fastener is fully damaged hence providing no restraint at all to the stud over its entire length (*L120_NoSprings*).

As shown in Fig.2, the stud has a strength of 58 kN at ambient temperature when considering the restraint from the sheathing. This strength is significantly larger than the demand on the stud at the beginning of the fire test, evaluated as either 2.9 kN (LC1) or 5.2 kN (LC2). If the sheathing restraint is fully lost, due to the prior shaking of the building, the strength is reduced to 14 kN. This major reduction shows the effect of sheathing restraint on the member strength. As the temperature increases, the cold-formed steel properties degrade, leading to a reduction of member strength. The member with full restraint from the sheathing fasteners has a critical temperature of about 850°C and 930°C for the loads of Load Case 2 and Load Case 1, respectively. Thus the stud, when fully supported, can withstand high temperatures, owing to the low demand over capacity ratio at ambient temperature. The unrestrained stud, however, has a critical temperature in the range of 600°C - 700°C. This evaluation provides useful insights into the buckling behavior and strength of the member under simplifying assumptions, including uniform temperature distribution. In the following section, FE analyses are conducted to analyze the nonlinear response of the CFS studs under transient nonuniform temperatures arising from the fire.

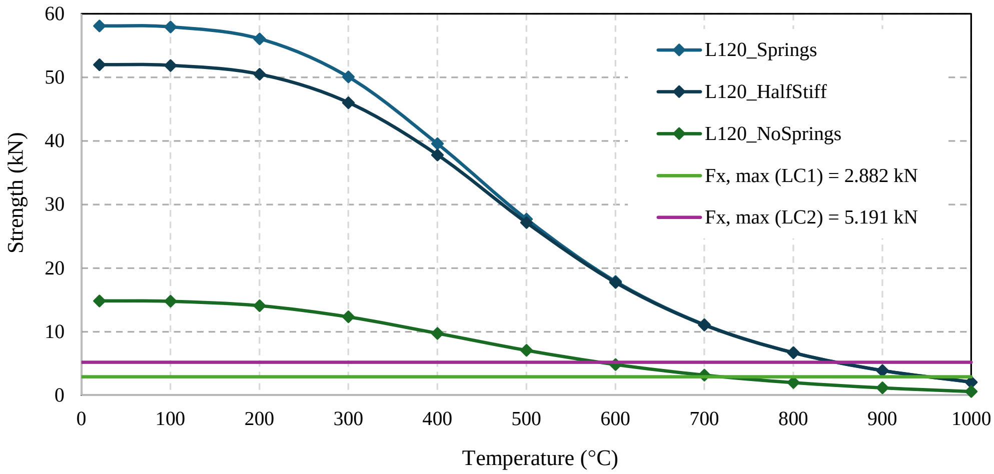

Fig. 2: Strength of the 600S162-54(50) stud in compression evaluated from the DSM as a function of temperature and stiffness from the sheathing fastener. Demand (axial force F_X) in the stud is also indicated.

3. Computational modeling framework

3.1. Software Integration: CUFSM and SAFIR

This work relies on the integration of the analysis tool CUFSM and the FE software SAFIR (Fig.3). CUFSM simplifies the modeling process by requiring only a cross-sectional representation of the member, enabling detailed analysis of cross-sectional instabilities and providing insights into buckling behavior. The results from CUFSM are then seamlessly integrated into SAFIR models using custom-developed Matlab scripts that directly connect the two software platforms and facilitate user inputs. SAFIR is a nonlinear FE software to model the thermal-mechanical response of structures under fire conditions (Franssen & Gernay, 2017).

For heat transfer modeling, additional user inputs such as fire scenarios, material thermal properties, sheathing conditions, and simulation time are used to construct SAFIR heat transfer models for CFS assemblies, including walls and floors. For thermal-mechanical modeling, the CUFSM outputs, including buckling analysis results, are combined with results from the SAFIR heat transfer analysis, such as temperature fields of the CFS members. These are further enhanced with additional user inputs, including geometrical imperfections derived from CUFSM analysis, material properties, boundary conditions, and simulation time, to generate models for transient or steady-state structural analysis. The effects of sheathing materials on the structural response can also be incorporated into the models using spring elements.

The seamless integration of CUFSM and SAFIR significantly enhances the modeling workflow, enabling rapid and comprehensive exploration of the thermal-mechanical behavior of cold-formed steel (CFS) systems, even under complex conditions such as nonuniform temperature distributions. For instance, in this study, which addresses multi-hazard scenarios, we investigate the varying damage states of sheathing resulting from earthquake events and examine their impacts on the thermal-mechanical responses of CFS members. This integrated approach facilitates a detailed analysis of how seismic damage influences the subsequent fire performance of CFS structures, thereby advancing our understanding of their resilience under combined hazards.

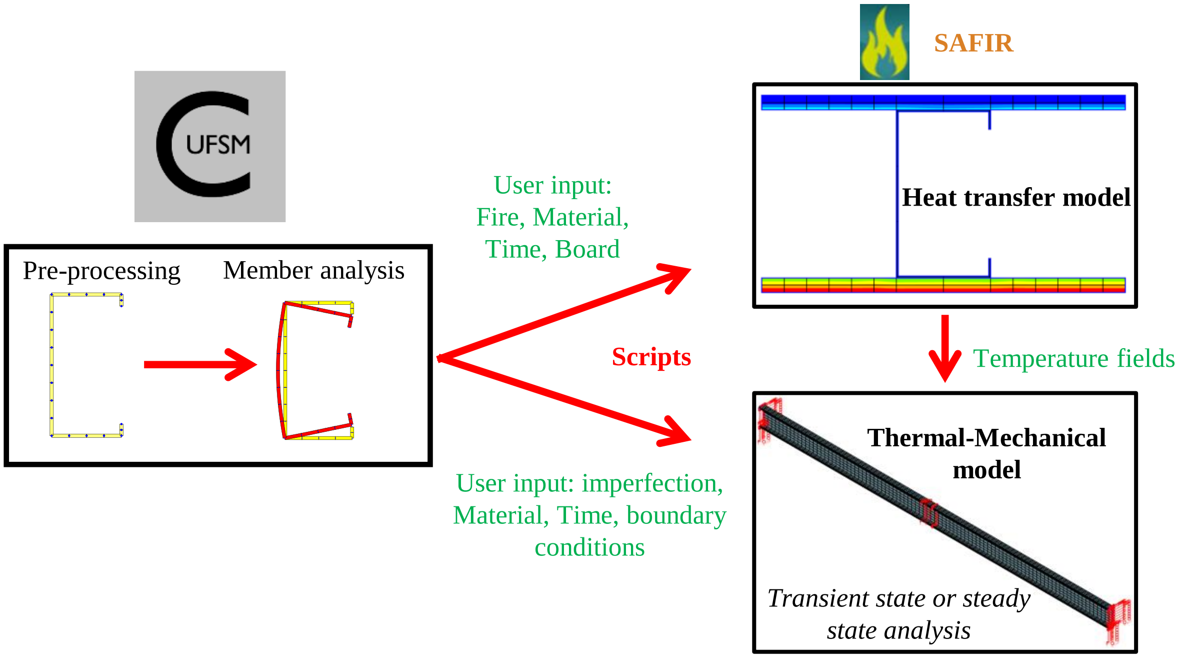

Fig. 3: Flowchart for the automatized CUFSM-SAFIR interfacing for CFS member analysis under fire.

3.2. Fire input

The fire modeling provides the input gas temperature-time curve for thermal analysis. The dimensions of the compartment (LxWxH) are 4.58 m x 6.71 m x 2.74 m. The compartment has four openings, three doors and one window. The doors will be shut during the fire test and the window will be broken prior to ignition to ensure safety of the shake table. The window will provide the major source of ventilation with an area of 1.7 m^2 (width = 1.22 m; height=1.42 m). Smaller amounts of leakages due to damage from the seismic tests will be present, but unaccounted for at this time since the damage is not known. Using the plot from Thomas and Heselden (1972) (Thomas & Heselden, 1972) the maximum compartment temperature during flashover is approximately 650°C using a ventilation factor of 44.0 $m^{-1/2}$.

The fuel for the compartment will be wood cribs uniformly spaced throughout the fire test compartment. The ventilation conditions of the compartment create a condition where the fully-developed heat release rate of the fire is expected to be 2.92 MW using the rate of air inflow through the window and the ambient oxygen levels (Drysdale, 2011). Different fire durations are considered for the fire test program. In this paper, a baseline case with a fully developed stage of the fire of 30 min is analyzed. The test program may consider longer fire durations, tentatively up to 60 min of fully developed stage, and analyses of these various exposures are ongoing. The amount of fuel (wood) placed within the compartment will be designed, based on the burning rate of the wood dependent on the ventilation conditions (Drysdale, 2011), to ensure the fully-developed fire lasts for the entire planned duration without prematurely entering the decay phase (fuel-controlled) of the compartment fire.

3.3 Thermal Modeling

2D thermal analyses are conducted in SAFIR on the 600S162-54 stud cross-section (Fig.4a). The analyses are run for two fire exposures: the ASTM E119 to evaluate the standard fire resistance

(*ASTM-E119*, 2018), and the natural fire with a fully developed phase at 650°C for 30 min (labeled *NatFire*). Additionally, the analyses consider various thickness of the gypsum plasterboard, including the intact thickness of 15.9 mm and degraded thicknesses of 10 mm and 5 mm, to capture in a simplified manner the effect of the possible prior damage to the sheathing from the pre-fire earthquake testing, which would influence the temperature increase in the studs. The gypsum board is meshed with 4 elements across the thickness. The stud is meshed with 20 elements along its cross-section to capture the nonuniform temperature distributions (Fig.4b). The thermal properties of the steel are taken from Eurocode EN1993-1–2 (*CEN, Eurocode 3: Design of Steel Structures - Part 1–2: General Rules - Structural Fire Design*, 2005). The Type X gypsum board, with a density as 648 kg/m^3 at ambient temperature, has temperature-dependent thermal properties taken from Cooper (Cooper, 1997).

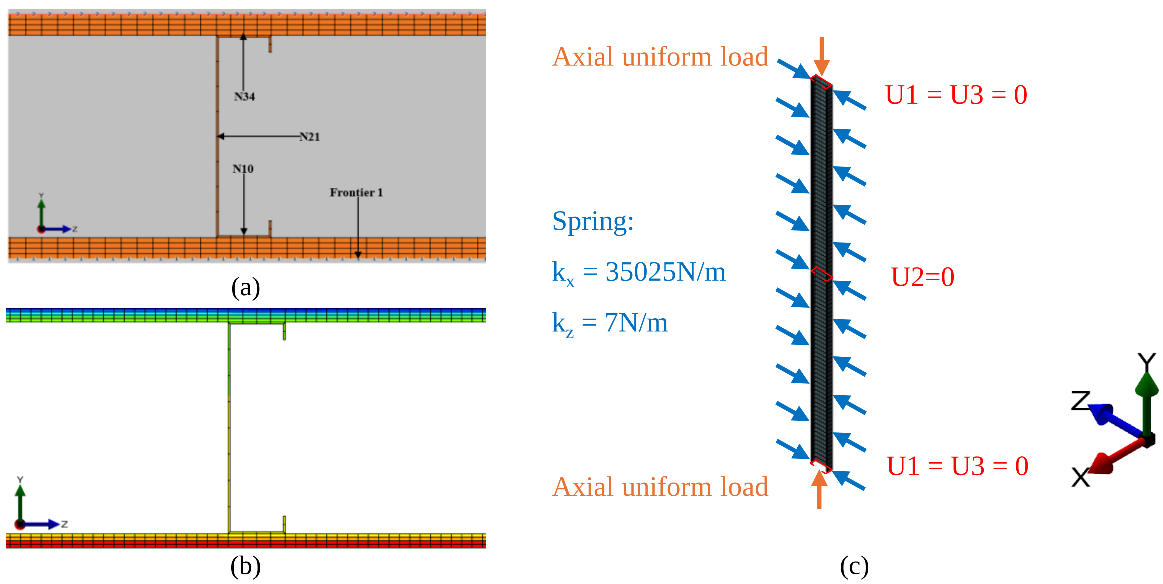

Fig. 4: Thermal-mechanical FE model of the stud. (a) Thermal model of the wall cross-section with node label. (b) Temperature distribution. (c) Structural analysis of the lipped channel in compression.

3.4. Structural Modeling

The lipped channels are modeled with quadrilateral shell elements in SAFIR (Fig.4c). Initial geometric imperfections derived from buckling mode shapes obtained using the finite strip method in CUFSM are incorporated into the model. Three different modes are considered for the imperfection distribution: a local buckling mode with a half-wavelength of 0.127 m and an amplitude of 0.34 times the plate thickness, a distortional buckling mode with a half-wavelength of 0.508 m and an amplitude of 0.94 times the plate thickness, and a global buckling mode with a half-wavelength of 3.048 m and an amplitude equal to the plate thickness (Schafer & Peköz, 1998). The steel modulus of elasticity is 203 GPa (29,500 ksi) and the yield strength is 345 MPa (50 kips). The stress-strain relationship is based on Von Mises plasticity with a softening branch and temperature-dependent properties. A mesh size between 6 and 33 mm is selected based on mesh sensitivity analysis. For boundary conditions, displacements parallel to the cross-sectional plane (x and z) are fixed at both ends, while the longitudinal displacement (y) is fixed at mid-height. Springs are used to simulate the restraints from the sheathing fasteners spaced at 304.8 mm with the same properties as used in the DSM of Section 2, including cases with half stiffness and no stiffness to capture seismic damage.

In this study, both transient state and steady-state analyses are conducted. In the transient state analysis, the load is applied first on the stud, and then (as the load is maintained constant) the temperature increases in the member. The temperature increase results from the thermal analysis discussed in Section 3.3. The analysis is run for 3 hours or until failure, whichever occurs first.

In the steady-state analysis, in contrast, a predefined temperature profile is applied first to the CFS member, and then the load is increased until failure (while the temperature is constant). Four temperature profiles are considered in the stud: (i) uniform temperature of 500°C, (ii) uniform temperature of 600°C, (iii) hot flange temperature of 500°C and cold flange of 330°C, (iv) hot flange temperature of 600°C and cold flange of 430°C. The 170°C gradient between the flange is selected from thermal analyses under typical conditions. The web temperature is taken as the average of the flanges. The analysis of a uniform temperature case allows comparison with the DSM results of Fig.2, and represents a limit case where the seismic shaking has led to complete loss of integrity of the gypsum sheathing, leading to direct hot gas exposure of the entire studs.

4. Parametric numerical analysis

4.1. Thermal response under various seismic damage

The temperature evolution in the CFS stud is plotted in Fig.5 under the two fire exposures and the three gypsum integrity conditions. Under the ASTM E119 fire, the stud temperature continuously increases over time. The temperature difference between the two flanges (N10 – N34) is also plotted. The rapid temperature rise in the early stage causes the temperature gradient between the flanges to initially increase, before decreasing and stabilizing in the later stage of the fire. Under the natural fire (NatFire), the stud temperature increases up to reaching a peak at approximately 30 minutes before starting to decrease as the fire decays. The peak temperature in the hot flange varies significantly with the thickness of the gypsum plasterboard, from about 300°C with the 15.9 mm thick gypsum (i.e., intact) to about 500°C with the 5 mm thick gypsum. After 3 hours, the temperatures of the flanges and the web drop below 80°C.

4.2. Time of failure under transient state analysis

The structural response of the stud is then evaluated under transient temperature conditions following the method described in Section 3.4. The stud is loaded with the LC2 force of 5191 N. The studied configurations along with their fire resistance times are summarized in Table 1. Under the ASTM E119 fire, the failure time ranges from 29 minutes to 98 minutes. The failure time decreases with a reduction in gypsum thickness, which could result from the pre-fire seismic tests. This is because the gypsum thickness influences the temperature distribution (Fig.5). For a given gypsum thickness, the presence of intermediate restraint along the length of the stud also influences the fire resistance. Indeed, the removal of the springs, which could occur from damage to the sheathing fasteners, leads to a substantial reduction in fire resistance time. Interestingly, reducing the stiffness of the support by 50% does not noticeably affect the fire resistance time of the studs. Under the natural fire, results suggest that the stud can survive the expected temperature-time exposure from the natural compartment fire, regardless of the tested assumptions on gypsum thickness and fastener restraint. This can be explained by the limited severity of the fire combined with the low demand over capacity ratio.

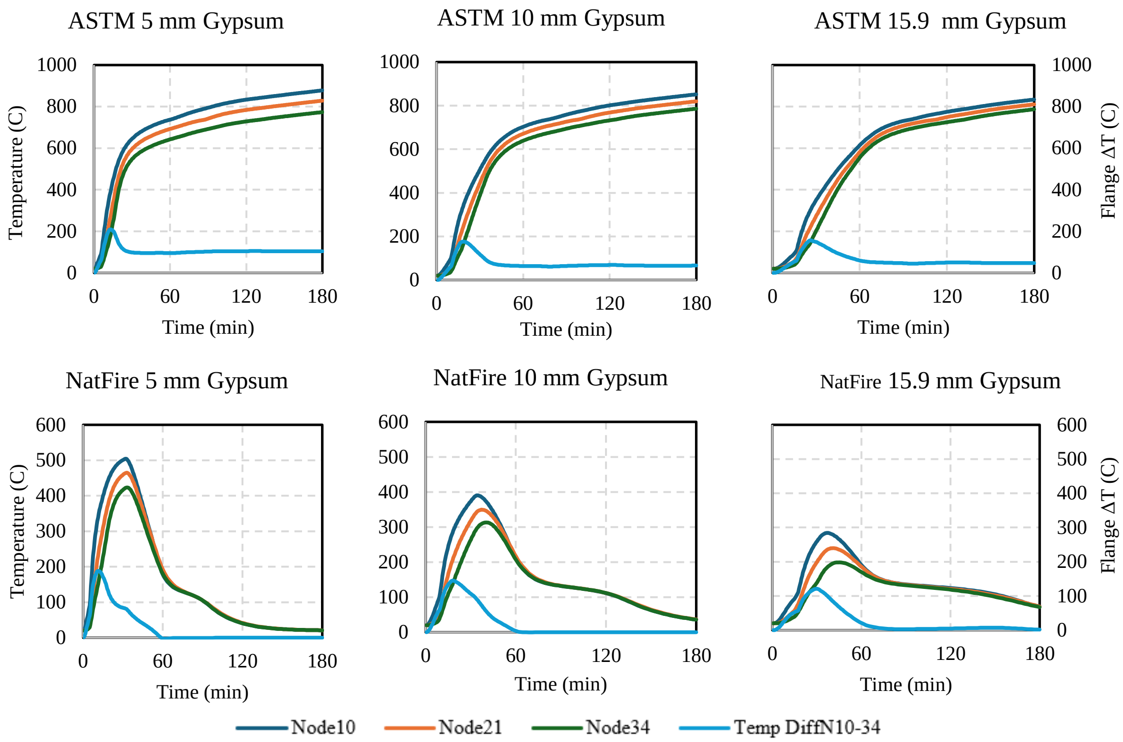

Fig. 5: Temperature distribution in the CFS stud.

Table 1. Parameters for the transient structural analysis and computed failure time.

Model	Section	Fire	Gypsum thick. (mm)	Fastener restraint	Failure time (min)
AS5F	600S162-54(50)	ASTM E119	5	Intact	72
AS10F	600S162-54(50)	ASTM E119	10	Intact	82
AS15.9F	600S162-54(50)	ASTM E119	15.9	Intact	93
AS5H	600S162-54(50)	ASTM E119	5	50% reduction	72
AS10H	600S162-54(50)	ASTM E119	10	50% reduction	82
AS15.9H	600S162-54(50)	ASTM E119	15.9	50% reduction	93
AS5N	600S162-54(50)	ASTM E119	5	Fully damaged	29
AS10N	600S162-54(50)	ASTM E119	10	Fully damaged	43
AS15.9N	600S162-54(50)	ASTM E119	15.9	Fully damaged	61
FM5F	600S162-54(50)	Natural Fire	5	Intact	no fail
FM10F	600S162-54(50)	Natural Fire	10	Intact	no fail
FM15.9F	600S162-54(50)	Natural Fire	15.9	Intact	no fail
FM5H	600S162-54(50)	Natural Fire	5	50% reduction	no fail
FM10H	600S162-54(50)	Natural Fire	10	50% reduction	no fail
FM15.9H	600S162-54(50)	Natural Fire	15.9	50% reduction	no fail
FM5N	600S162-54(50)	Natural Fire	5	Fully damaged	no fail
FM10N	600S162-54(50)	Natural Fire	10	Fully damaged	no fail
FM15.9N	600S162-54(50)	Natural Fire	15.9	Fully damaged	no fail

Variation of the sheathing restraint influences not only the fire resistance time but also the buckling mode. For example, Fig.6 shows the deformed shape at failure for the stud with 5 mm gypsum thickness subjected to the ASTM E119 fire. The member with sheathing fastener restraint intact fails after 72 minutes by local web buckling. This behavior occurs because the springs provide stiffness restraining deformation in the direction parallel to the flanges. In contrast, the member with fully damaged fasteners has no springs in the model, and therefore is subject to global buckling and twisting. This member fails after 29 minutes by flexural-torsional buckling.

The transient analyses capture the thermal bowing of the members from the nonuniform temperature distribution. The maximum temperature difference between the flanges may reach up to 200°C. This temperature difference induces uneven deformation in the stud, as the thermal expansion of one flange is larger than that of the other flange. This results in thermal bowing of the stud toward the fire. Additionally, the degradation of the mechanical properties is also nonuniform across the section. These complex effects are captured by the analysis and influence the stability and strength of the member during the fire exposure.

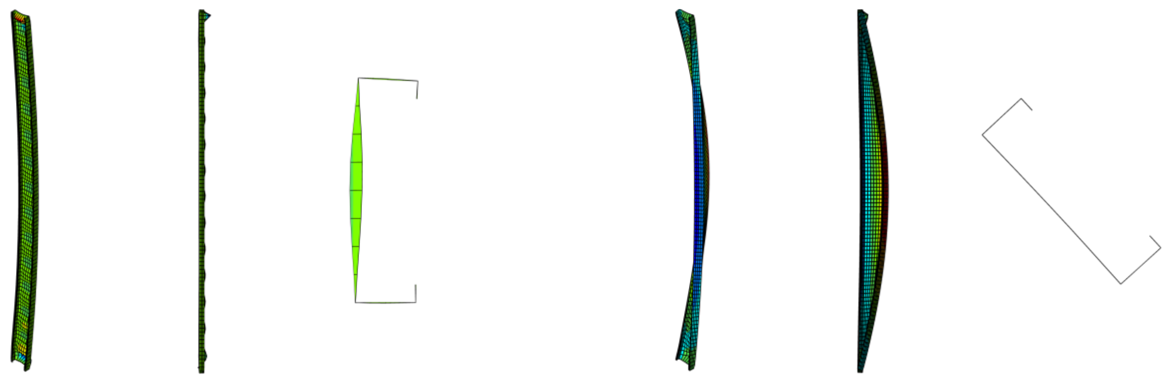

(a) fastener restraint intact (b) fully damaged fastener restraint

Fig. 6: Deflected shape at failure for AS5F and AS5N (magnification factor 10)

4.3. Load-bearing capacity under steady-state nonuniform temperature

The structural response of the studs is also evaluated under steady-state temperatures, as discussed in Section 3.4. In this regime, a temperature distribution is first applied to the stud, followed by loading up to failure. The studied configurations and resulting computed member strength are listed in Table 2.

Results show that the higher the stud temperature, the lower its load-bearing capacity. This is expected under uniform temperature distribution, i.e., the strength of the stud is obviously lower at 600°C than at 500°C. But this is also the case under nonuniform temperature, i.e., the stud with one hot flange and one cooler flange (e.g., 500°C and 330°C) has a higher strength than the stud with two hot flanges (500°C). This result indicates that, for the studied configurations, the detrimental effect of thermal gradient does not prevail over the effect of reduced material properties. It also means that it would be overly conservative to evaluate the strength of the stud under nonuniform temperatures based on the hot flange temperature only, as is sometimes done with simplified methods.

Reducing by half the stiffness provided by the sheathing fasteners does not significantly affect the load-bearing capacity of the studs. However, the load-bearing capacity of the studs decreases significantly when this restraint is fully removed, which aligns with the conclusions drawn from the DSM analysis (Fig.2) and the transient state analysis (Table 1). The findings emphasize that a loss of integrity of these sheathing-to-stud connections from the seismic shaking would greatly affect the load-bearing capacity under elevated temperatures.

Importantly, the analyses suggest that no failure would be expected as long as the maximum temperature in the stud does not exceed 600°C during the fire test. Indeed, the load-bearing capacity reaches a minimum of 5.5 kN under the most severe assumption of absence of restraint along the stud due to gypsum integrity failure after seismic testing. This member strength is still higher than the load of 5.2 kN evaluated based on the load combination LC2 (see Section 2).

Table 2. Parameters for the steady-state structural analysis and computed strength.

Model	Section	T (°C)	Fastener restraint	Strength (kN)
U500F	600S162-54(50)	Uniform500	Intact	24.7
U500H	600S162-54(50)	Uniform500	50%	24.7
U500N	600S162-54(50)	Uniform500	0%	8.0
U500W415L330F	600S162-54(50)	UFlange500Web415LFlange330	Intact	33.7
U500W415L330H	600S162-54(50)	UFlange500Web415LFlange330	50%	33.7
U500W415L330N	600S162-54(50)	UFlange500Web415LFlange330	0%	9.2
U600F	600S162-54(50)	Uniform600	Intact	15.9
U600H	600S162-54(50)	Uniform600	50%	15.9
U600N	600S162-54(50)	Uniform600	0%	5.5
U600W515L430F	600S162-54(50)	UFlange600Web515LFlange430	Intact	23.1
U600W515L430H	600S162-54(50)	UFlange600Web515LFlange430	50%	23.1
U600W515L430N	600S162-54(50)	UFlange600Web515LFlange430	0%	6.5

5. Conclusion and future works

This study investigated the post-earthquake fire performance of load-bearing cold-formed steel studs in the 10-story CFS building that will be tested on the NHERI LHPOST6 at UC San Diego in 2025. A computational modeling framework was developed combining the elastic buckling analysis software CUFSM and the nonlinear thermal-mechanical finite element software SAFIR. The main findings are summarized hereafter.

- There is agreement between the Direct Strength Method and the SAFIR finite element model in terms of evaluation of the stud strength under uniform elevated temperature. For the stud with full restraint from the sheathing, the DSM and SAFIR provide strengths of 28 kN and 25 kN at 500°C, respectively, and of 18 kN and 16 kN at 600°C, respectively. From the DSM analysis, the critical temperature of the stud under the fire design load combination is 850°C with full sheathing fastener restraint and 600°C in the absence of such restraint.

- The developed computational framework allows capturing transient nonuniform temperature histories from fire exposure in the cold-formed steel member. Under the baseline compartment fire with a fully developed phase of 30 min, the transient analysis indicates that the studs are not expected to fail, owing to the low demand over capacity ratio in the stud (hence their high critical temperature) and the moderate severity of the fire, which peaks at 650°C. Longer fire durations are under consideration for the test program and will be studied next.

- Both transient and steady-state analyses reveal the significance of the gypsum board in enhancing the fire performance of the cold-formed steel shear walls through both thermal insulation and restraint of global flexural-torsional buckling. Pre-fire seismic damage to the gypsum and its fasteners have the potential to significantly reduce the thermal-mechanical performance of the studs. Under unfavorable conditions of complete loss of fastener restraint and temperature in the stud reaching 600°C, the strength is reduced to 5.5 kN, which still exceeds (but barely) the force of 5.2 kN resulting from the fire design load combination. The stud without the support of the sheathing fasteners could thus collapse if exposed to higher temperature compartment fires.

The pre-test modeling efforts described in this paper will be continued to further inform the planning of the CFS-NHERI building test program, including further analyses of members in the load-bearing wall and floor assemblies and different fire scenarios. After the experiments, the collected data will then be used to refine and validate the numerical models, enhancing their accuracy in predicting post-earthquake fire performance, and for running parametric analyses. The results from these tests and simulations will serve to improve performance-based fire design guidelines for cold-formed steel structures including under multi-hazard scenarios.

Acknowledgment
This research was supported by the National Science Foundation (NSF) through award #2237623 "CAREER: Performance-Based Fire Design for Cold-Formed Steel Structures" (PI T. Gernay, Program Manager J. Pauschke, CMMI). The financial support is gratefully acknowledged. The authors thank PhD student Mohammed Eladly and Prof. Ben Schafer for providing the input forces from the ambient temperature numerical model.

References

Abreu, J. C. B., Vieira Jr, L. C., Moreno Jr, A. L., Gernay, T., & Schafer, B. W. (2020). Experiments on load-bearing cold-formed steel sheathed studs at elevated temperatures. *Thin-Walled Structures*, *156*, 106968.

Adany, S. (2006). Buckling Analysis of Cold-formed Steel Members Using CUFSM: Conventional and Constrained Finite Strip Methods. *CCFSS Proceedings of International SpecialtyConference on Cold-Formed Steel Structures(1971-2018)*. (2006)-18th International Specialty Conferenceon Cold-Formed Steel Structures.

Castaneda, H. (2022). *Seismic performance of cold-formed steel diaphragms*. University of Massachusetts.

CEN, Eurocode 3: Design of Steel Structures—Part 1–2: General Rules—Structural Fire Design. (2005).

CFS-NHERI: 10-Story Building Capstone Test Program. (2025). https://cfs10.ucsd.edu

Chen, W., Ye, J., Zhao, Q., & Jiang, J. (2020). Full-scale experiments of gypsum-sheathed cavity-insulated cold-formed steel walls under different fire conditions. *Journal of Constructional Steel Research*, *164*, 105809.

Cooper, L. Y. (1997). *The Thermal Response of Gypsum-panel/steel-stud Wall Systems Exposed to Fire Environments: A Simulation for Use in Zone-type Fire Models*. National Bureau of Standards. https://firedoc.nist.gov/article/KXcyXYQBWEcjUZEYyMbP

Drysdale, D. (2011). *An Introduction to Fire Dynamics (3rd edition)*. John Wiley and Sons.

Feng, M., & Wang, Y.-C. (2005). An experimental study of loaded full-scale cold-formed thin-walled steel structural panels under fire conditions. *Fire Safety Journal*, *40*(1), 43–63.

Franssen, J.-M., & Gernay, T. (2017). Modeling structures in fire with SAFIR®: Theoretical background and capabilities. *Journal of Structural Fire Engineering*, *8*(3), 300–323.

Hutchinson, T. C., Wang, X., Hegemier, G., Kamath, P., & Meacham, B. (2021). Earthquake and Postearthquake Fire Testing of a Midrise Cold-Formed Steel-Framed Building. I: Building Response and Physical Damage. *Journal of Structural Engineering*, *147*(9), 04021125. https://doi.org/10.1061/(ASCE)ST.1943-541X.0003097

Kamath, P., Meacham, B. J., Wang, X., & Hutchinson, T. C. (2017). *Full-Scale Fire Tests on a Cold-Formed Steel Frame in Fire Following Earthquake*. IFireSS 2017 – 2nd International Fire Safety Symposium, Naples, Italy.

Li, Z., & Schafer, B. (2010). Buckling Analysis of Cold-formed Steel Members with General Boundary Conditions Using CUFSM Conventional and Constrained Finite Strip Methods. *CCFSS Proceedings of International Specialty Conference on Cold-Formed Steel Structures (1971 - 2018)*. 20th International Specialty Conference on Cold-Formed Steel Structures. https://scholarsmine.mst.edu/isccss/20iccfss/20iccfss-session1/2

Liu, P., Peterman, K. D., & Schafer, B. W. (2014). Impact of construction details on OSB-sheathed cold-formed steel framed shear walls. *Journal of Constructional Steel Research*, *101*, 114–123.

Meacham, B. J. (2016). Post-Earthquake Fire Performance of Buildings: Summary of a Large-Scale Experiment and Conceptual Framework for Integrated Performance-Based Seismic and Fire Design. *Fire Technology*, *52*(4), 1133–1157. https://doi.org/10.1007/s10694-015-0523-9

Miller, T. H., & Pekoz, T. (1993). Behavior of Cold-Formed Steel Wall Stud Assemblies. *Journal of Structural Engineering*, *119*(2), 641–651. https://doi.org/10.1061/(ASCE)0733-9445(1993)119:2(641)

Ni, S., Yan, X., Hoehler, M. S., & Gernay, T. (2022). Numerical modeling of the post-fire performance of strap-braced cold-formed steel shear walls. *Thin-Walled Structures*, *171*, 108733.

Peterman, K. D., & Schafer, B. W. (2012). Stability of sheathed cold-formed steel studs under axial load and bending. *Proceedings of the Annual Stability Conference, Structural Stability Research Council. Dallas, TX*. https://www.aisc.org/globalassets/continuing-education/ssrc-proceedings/2012/stability-of-sheathed-cold-formed-steel-studs-under-axial-load-and-bending.pdf

Peterman, K. D., & Schafer, B. W. (2014). Sheathed Cold-Formed Steel Studs under Axial and Lateral Load. *Journal of Structural Engineering*, *140*(10), 04014074. https://doi.org/10.1061/(ASCE)ST.1943-541X.0000966

Peterman, K. D., Stehman, M. J. J., Madsen, R. L., Buonopane, S. G., Nakata, N., & Schafer, B. W. (2016). Experimental Seismic Response of a Full-Scale Cold-Formed Steel-Framed Building. I: System-Level Response. *Journal of Structural Engineering*, *142*(12), 04016127. https://doi.org/10.1061/(ASCE)ST.1943-541X.0001577

Schafer, B. W. (2008). The direct strength method of cold-formed steel member design. *Journal of Constructional Steel Research*, *64*(7–8), 766–778.

Schafer, B. W., & Peköz, T. (1998). Computational modeling of cold-formed steel: Characterizing geometric imperfections and residual stresses. *Journal of Constructional Steel Research*, *47*(3), 193–210.

Singh, A., Wang, X., Zhang, Z., Derveni, F., Castaneda, H., Peterman, K. D., Schafer, B. W., & Hutchinson, T. C. (2022a). Steel Sheet Sheathed Cold-Formed Steel Framed In-line Wall Systems. I: Impact of Structural Detailing. *Journal of Structural Engineering*, *148*(12), 04022193. https://doi.org/10.1061/(ASCE)ST.1943-541X.0003433

Singh, A., Wang, X., Zhang, Z., Derveni, F., Castaneda, H., Peterman, K. D., Schafer, B. W., & Hutchinson, T. C. (2022b). Steel Sheet Sheathed Cold-Formed Steel Framed In-line Wall Systems. II: Impact of Nonstructural Detailing. *Journal of Structural Engineering*, *148*(12), 04022194. https://doi.org/10.1061/(ASCE)ST.1943-541X.0003434

Thomas, P. H., & Heselden, A. J. M. (1972). *Fully-developed Fires in Single Compartments: A Co-operative Research Programme of the Conseil International Du Batiment*. Fire Research Station.

Vieira Jr, L. C. M., Shifferaw, Y., & Schafer, B. W. (2011). Experiments on sheathed cold-formed steel studs in compression. *Journal of Constructional Steel Research*, *67*(10), 1554–1566.

Vieira Jr, L. C., & Schafer, B. W. (2012). Lateral stiffness and strength of sheathing braced cold-formed steel stud walls. *Engineering Structures*, *37*, 205–213.

Vy, S. T., Mahendran, M., Steau, E., & Ariyanayagam, A. (2023). Full-scale tests of load-bearing LSF walls made of built-up CFS channel sections under fire conditions. *Thin-Walled Structures*, *187*, 110763.

Washington (DC, USA), ASCE/SEI 7-22, Minimum Design Loads and Associated Criteria for Buildings and Other Structures, American Society of Civil Engineers. (2022).

West Conshohocken (PA, USA), ASTM-E119-18c, Standard Test Methods for Fire Tests of Building Construction and Materials. (2018).

Yan, X., Abreu, J. C. B., Glauz, R. S., Schafer, B. W., & Gernay, T. (2021). Simple Three-Coefficient Equation for Temperature-Dependent Mechanical Properties of Cold-Formed Steels. *Journal of Structural Engineering*, *147*(4), 04021035. https://doi.org/10.1061/(ASCE)ST.1943-541X.0002990

Yan, X., & Gernay, T. (2022). Structural fire design of load-bearing cold-formed steel assemblies from a prototype metal building. *Structures*, *41*, 1266–1277. https://doi.org/10.1016/j.istruc.2022.05.078

Ye, J., Wang, X., Jia, H., & Zhao, M. (2015). Cyclic performance of cold-formed steel shear walls sheathed with double-layer wallboards on both sides. *Thin-Walled Structures*, *92*, 146–159.

Zhang, Z., Eladly, M. M., Rogers, C. A., & Schafer, B. W. (2024). Cold-formed steel framed shear wall test database. *Earthquake Spectra*, *40*(1), 871–884. https://doi.org/10.1177/87552930231202974

Zhang, Z., Singh, A., Derveni, F., Torabian, S., Peterman, K. D., Hutchinson, T. C., & Schafer, B. W. (2022). Cyclic Experiments on Steel Sheet Connections for Standard CFS Framed Steel Sheet Sheathed Shear Walls. *Journal of Structural Engineering*, *148*(2), 04021261. https://doi.org/10.1061/(ASCE)ST.1943-541X.0003233